HHS Public Access

Author manuscript

J Alzheimers Dis. Author manuscript; available in PMC 2015 May 06.

Published in final edited form as:

J Alzheimers Dis. 2014 ; 42(1): 333–344. doi:10.3233/JAD-140252.

Determination of Small Molecule ABAD Inhibitors Crossing Blood Brain Barrier and Pharmacokinetics

Jhansi Rani Vangavaragu[a], **Koteswara Rao Valasani**[a], **Du Fang**[a], **Todd D. Williams**[b], and **Shirley ShiDu Yan**[a,*]

[a]Department of Pharmacology & Toxicology, Higuchi Bioscience Center, School of Pharmacy, University of Kansas, Lawrence KS 66044, USA

[b]Mass Spectrometry Laboratory University of Kansas, Lawrence KS 66047, USA

Abstract

A major obstacle to the development of effective treatment of Alzheimer's disease (AD) is successfully delivery of drugs to the brain. We have previously identified a series of benzothiazole phosphonate compounds that block the interaction of amyloid beta peptide (Aβ) with amyloid-beta binding alcohol dehydrogenase (ABAD). A selective and sensitive method for the presence of three new benzothiazole ABAD inhibitors in mouse plasma, brain and artificial cerebrospinal fluid has been developed and validated based on high performance liquid chromatography tandem mass spectrometry. Mass spectra were generated using Micromass Quattro Ultima "triple" quadrupole mass spectrometer equipped with Electrospray ionization interface. Good linearity was obtained over a concentration range of 0.05–2.5 μg/ml. The lowest limit of quantification and detection was 0.05μg/ml. All inter-day accuracies and precisions were within ±15% of the nominal value and ±20%, respectively, at the lower limit of quantitation. The tested compounds were stable at various conditions with recoveries >90.0 % (RSD<10%). The method used for pharmacokinetic studies of compounds in mouse cerebrospinal fluid, plasma, and brain is accurate, precise, and specific with no matrix effect. Pharmacokinetic data showed these compounds penetrate the blood–brain barrier (BBB) yielding 4–50 ng/ml peak brain concentrations and 2 μg/ml peak plasma concentrations from a 10mg/kg dose. These results indicate that our newly synthesized small molecule ABAD inhibitor have good drug properties with the ability to cross the blood brain barrier, which holds a great potential for AD therapy.

Keywords

ABAD inhibitors; amyloid-β; benzothiazole phosphonates; blood-brain barrier pharmacokinetics

INTRODUCTION

Accumulation of the toxic amyloid-beta peptide (Aβ) in the brain is considered to be one of the primary causes for the Alzheimer's disease (AD) pathogenesis. Mitochondria and synaptic dysfunction is an early pathological feature of AD affected brain [1–6], with Aβ

*Corresponding author: Shirley S. Yan, 2099 Constant Avenue, University of Kansas, Lawrence, KS 66047. shidu@ku.edu, Tel: (785) 864-4002 | Fax: (785) 864-5219.

progressively accumulating in synaptic mitochondria and impairing mitochondrial structure and function including membrane potential, membrane permeability transition pore, respiration, energy metabolism, oxidative stress, mitochondrial dynamics, energy metabolism and calcium homeostasis [7–16]. Aβ binding alcohol dehydrogenase (ABAD) is a mitochondrial enzyme essential for metabolic function within the mitochondria [17–24]. Since Aβ forms a complex with ABAD, this enzyme has gained considerable interest as a potential target for AD treatment. More specifically, prevention and treatment of AD could perhaps be accomplished through the development of molecules that inhibit the formation of the Aβ-ABAD complex or compounds that block Aβ production.

Recent studies indicate that Aβ toxicity may be linked to the mitochondrial dysfunction present in AD [7, 15, 16, 25–29]. Through this interaction, Aβ is able to suppress normal ABAD enzymatic activity [30], while promoting oxidative stress[15, 25] and triggering a signal cascade resulting in apoptosis[15, 25]. Structural studies [15, 26] of this interaction show that introduction of Aβ results in a conformational change in ABAD preventing the binding of NAD^+ and the loss of ABAD enzymatic activity. Targeted interruption of Aβ-ABAD binding has been shown to suppress Aβ-induced neuronal dysfunction, which suggests that the Aβ-ABAD interaction is a prime target for novel AD treatment [22, 23]. The search has already started for inhibitors of this interaction with the most promising treatments being derived from the class of benzothiazolyl ureas [31].

Frentizole is a nontoxic antiviral and immunosuppressive benzothiazolyl urea drug [31], approved by the Food and Drug Administration (FDA) for rheumatoid arthritis and systemic lupus erythematosus. We identified frentizole as a novel inhibitor of the Aβ–ABAD interaction using ELISA-based screening assays for 45 benzothiazole urea compounds[31]. A novel benzothiazole urea with a 30-fold improvement in potency was identified from analysis of the frentizole structure–activity relationship (SAR) [31]. The SAR studies indicated that small electron-withdrawing groups were desirable as substituents on the benzothiazole ring and compounds with a hydroxyl group at the para position of the phenyl ring were particularly potent. In order for these compounds to readily penetrate the blood-brain barrier (BBB) and enter the target organ [32–34], these compounds were converted to benzothiazole phosphonates. Since water solubility is essential, phosphate esters are frequently used as a prodrug strategy. The properties of xenobiotics can be enhanced in several ways by incorporating phosphate groups. Phosphate groups increase water solubility and thereby enable parenteral drug delivery. Phosphate groups can sometimes decrease the adverse effects of drugs and they can also provide significant and sustained delivery of the active drug species to the target organ by *in vivo* cleavage of the phosphonate carrier/drug linkage to provide a hydrophilic, negatively charged intermediate, which is ’locked’ in the brain or other organ[32–36]. Three potent benzothiazole phosphonate inhibitors of the ABAD-Aβ interaction (A1, A5 and A6) that bind to ABAD were identified using these criteria [37], they also rescued Aβ-mediated mitochondrial dysfunction [38]. These compounds are therefore potential therapeutic treatments for AD and their pharmacokinetic profile needs to be assessed. Currently, there are no data on the *in vivo* pharmacokinetic behavior of these compounds. Thus, there is a need to develop reliable analytical methods for evaluating the properties of these inhibitors. Liquid chromatography tandem mass

spectrometry (LC-MS/MS) is a proven method for the analysis of chemical compounds and can provide the low detection limits needed for compounds of interest.

The aim of this study is to validate a LC-MS/MS method of analysis with high sensitivity and reliability for the routine analysis of our compounds in mouse plasma and brain. Our objective is to build a pharmacokinetic profile and assess the ability of compounds A1, A5 and A6 to cross the BBB in mice after intravenous administration.

MATERIALS AND METHODS

Chemical and reagents

Benzothiazole amino phosphonate derivatives were synthesized using a three-component reaction of equimolar quantities of aromatic aldehydes, 6-methoxybenzo[d]thiazol-2-amine, and dimethyl phosphate in toluene at reflux temperature in the presence of $Mg(ClO_4)_2$ [37]. In this study, we examined the three compounds that show better biological activity based on binding affinity and effect on mitochondrial function induced by calcium or Aβ [38]. Compounds A1, A5 and A6 were in the form of white powder characterized by melting points of 216 °C, 180 °C, 178 °C and exact masses of 453.0881 ± 0.0004 (n = 5) 0.1 ppm, 395.0819 ± 0.0006 (n = 3) 3.0 ppm and 397.0788 ± 0.0012 (n = 3) 0.3 ppm, respectively. The molecular formula for A1, A5, and A6 are $C_{19}H_{22}N_2O_7PS$, $C_{17}H_{19}N_2O_5PS$, and $C_{17}H_{19}FN_2O_4PS$ (Figure 1). The purity of the compounds was greater than 99% using HPLC. A sample of 800 nM concentration of each compound gave a chromatogram with S/N>100 with was no other detectable peak. HPLC grade methanol, ethanol, formic acid, sodium chloride, potassium chloride, calcium chloride, magnesium chloride, HEPES, monosodium phosphate and sodium bicarbonate were purchased from Sigma (USA). A Millipore purification system (Labconco, Kansas City, MO, USA) was used to provide Millipore water.

Instrumentation—A Waters Acquity “classic” UPLC (Waters Corp USA) was used to develop CH_3CN gradients on a C-18 reverse phase column. Column- effluent was introduced to the electrospray source of a Micromass Quattro Ultima “triple” quadrupole mass spectrometer (Micromass Ltd., Manchester, UK).

Methods

LC method for MS detection—Chromatographic separation was on an ACE C18 column (Mac Mod Analytical, 3μm, Ultra-Inert HPLC Column, 50×2.1mm) protected by a matched ACE guard cartridge. Separation solvents were A: H_2O (99%), methanol (1%) and formic acid (0.1%) and B: H_2O (1%), methanol (99%) and formic acid (0.1%) delivered at a flow rate of 400 μl/min. The hydrophobic character of the analytes allows a large injection (50 μl) to chromatofocus on a column at 5% B. After 0.2 min, separation was with a linear gradient of 11% B/min for 4 min. Column wash was to 80% B for 2 min and re-equilibration at 5% B for 1.5 min for a total run-time of 8 min. The first 2 min of chromatographic effluent was diverted to waste.

Mass spectrometry parameters—The mass spectrometer was run in positive ion mode using the electrospray ionization (ESI) source. The source block was 100°C and desolvation gas temperature 300°C. Argon collision gas pressure on a line to the cell was 1E-3 mbar. Quadrupoles 1 and 3 were set to 0.9 amu FWHH. Collision energy and cone voltage settings were optimized for each compound. The data were processed using MassLynx 4.1/ QuanLynx and Graphpad Prism 5. Fragmentation patterns of compounds A1, A5, and A6, methyl (Z)-3-(((6-methoxybenzo[d]thiazol-2-yl)imino)methyl)benzoate, 4-(1-((6-methoxybenzo- [d]thiazol-2-yl) amino) ethyl) phenol and (Z)-1-(4-fluorophenyl)-N-(6-methoxybenzo[d]thiazol-2-yl) methanimine were determined by infusing an aqueous/ methanol solution introduce with a T fitting into 30% solvent B from the UPLC for source optimization. The most abundant transitions were chosen for all the three compounds (Fig. 1).

Preparation of calibration standards for recovery and quality controls—Stock solutions of A1, A5 & A6 and internal standards (IS) of 1mM in methanol were used to create calibration standards. Fifty microliters of IS (1μg/ml) plus 50 μl of calibration standard were diluted with 100 μl of water for a curve of nominal concentrations 0.05 to 2.5 μg/ml to be injected onto the LC column. Quality control samples were prepared at nominal concentrations of low (0.05 μg/ml), medium (0.875 μg/ml), and high (2.5 μg/ml).

Preparation of calibration standards in matrices and quality controls samples —Calibration standards were prepared by spiking into 50 μl of blank plasma, brain or artificial cerebrospinal fluid (ACSF) to yield final concentrations of 0.05 to 2.5 μg/ml. Quality control (QC) samples were prepared in the same manner at concentrations of 0.05, 0.875 and 2.5 μg/ml for the low, medium and high level.

Sample preparation

ACSF Sample preparation: Due to the modest volume of CSF available from a mouse i.e., approximately 5 μl per mouse, we have selected an ACSF for development and calibration. The ACSF consists of 126 mM NaCl, 2.5 mM KCl, 20 mM HEPES, 1.2 mM NaH_2PO_4, 25 mM $NaHCO_3$, 2.4 mM $CaCl_2$, and 1.2 mM $MgCl_2$ at pH 7. Calibration points were 50μl of IS (1μg/ml), 50μl of calibration standard and the mixture then diluted with 100μl of ACSF, yielding final concentrations of IS (0.5 μg/ml) & standard sample (0.05–2.5 μg/ml) such that 50% organic and 50% ACSF solution were injected onto the LC.

Plasma Sample preparation: Mouse plasma samples, 50 μl, were transferred to a 1.5 ml centrifuge tube and then 50 μL of IS (4 μg/ml) and 50μL of calibration standard sample were vortexed for 30 s. Acetonitrile (0.1ml) was added to precipitate the proteins. After being vortexed for 3min, the sample was centrifuged for 10min at 13000 rpm. Supernatant (50 μl) was diluted with 50 μl water and injected onto the column.

Brain Sample preparation: Brain tissue 100 mg was weighed and placed in a centrifuge tube. Methanol (100 μl) was added and homogenized for 1min before adding 100 μl IS (6 μg/ml) to the homogenized mixture. The sample was vortexed for 30 s before centrifuging for 10 min at 13000 rpm. Then supernatant liquid was diluted 50% with water and injected.

Method validation: The developed method was validated in terms of selectivity, linearity, lower limits of quantification (LLOQ), accuracy, precision, recovery, stability and matrix effects according to the FDA guidelines [39].

Accuracy and precision: Intra-day accuracy was calculated by using replicates (n = 5) of A1, A5 and A6 at three concentrations 0.05, 0.875 and 2.5 μg/ml of the spiked matrices during a single analytical session. The inter-day precision was also assessed by using replicates (n = 5) of three concentrations made on three separate days.

Stability: The stability of compounds A1, A5 and A6 was evaluated in ACSF, plasma and brain matrices under various temperature and storage conditions. Stability at room temperature was examined by analyzing samples at 25°C for 2 and 4 h and stability at −80°C was checked for one month. Samples were analyzed after three freeze-thaw cycles (−80°C to 25°C). Stability studies were performed at three concentrations.

Matrix effects assessment: Matrix effects were assessed with a post column infusion method. A pump infused each analyte at low concentration at a constant rate into a T fitting post column. The spectrometer was set to SRM mode for that target. Sample preparations, without analyte, were resolved on the LC column.

Extraction Recovery: The extraction recovery of each analysis was determined at the three concentrations low, mid and high (0.05, 0.875, and 2.5 μg/ml) using the non-dosed ACSF, plasma and brain samples. To determine the recovery, signals of spiked extracts from the blank ACSF, brain and plasma were compared with that of injection of pure standards in mobile phase. IS recovery was determined for a single concentration of 0.5 μg/ml.

Linearity and LLOQ: A calibration curve was prepared from a plot of the peak area ratio (y) of each analyte to IS against plasma concentration (x) using weighted (1/x) least squares regression analysis.

Application to pharmacokinetic study and data analysis: This study was performed in accordance with the recommendations in the Guide for the Care and Use of Laboratory Animals of the National Institutes of Health. Animal studies were approved by the Animal Care and Use Committee of University of Kansas in accordance with the National Institutes of Health guidelines for animal care. Using the validated LC-MS/MS method, blood and brain levels A1, A5 and A6 were measured in male and female C57BL6 mice (8-week-old, weighing approximately 25–30 g). The mice were housed in a room with controlled temperature (23 ± 3°C) and moisture level (55 ± 15% relative humidity) and exposed to a controlled 12 h light/12 h dark cycle. They were allowed to access to food and water *ad libitum*. Mice were fasted for 6h with free access to water prior to the pharmacokinetic study. To determine the time course of compounds A1, A5 and A6 action in the brain, we investigated the plasma pharmacokinetics and BBB penetration capability of the inhibitors. In these experiments, A1, A5 and A6 were administered to mice by intravenous injection at a dosage of 10 mg/kg. Blood and brain samples were collected from mouse at each time point (2, 5, 10, 30, 60, 120, 240, 360, 720, 1440 and 2880min), a total of 11 time points. For plasma measurements, blood (approximately 500–800 μl) was collected via cardiac–

puncture into tubes containing sodium heparin anti-coagulant. Plasma was separated via centrifugation (4°C, 3500 rpm, 10 min) and stored in −80°C freezer. Qualitative confirmations of these compounds in CSF; samples were collected at 2 time points (240 and 1440min) from five animals at each time points. At the time of measurement, frozen plasma samples were thawed at room temperature and vortexed thoroughly. The following quantities were estimates using non-compartmental calculations performed with WinNonlin™ 5.2 (Pharsight, Sunyvale, CA): 1) The area under the plasma concentration-time curve during the period of observation ($AUC_{0\text{-}t}$); 2) The area under the plasma concentration-time curve from zero to infinity ($AUC_{0\text{-}\infty}$); 3) The maximum plasma concentration (C_{max}); 4) The time to reach C_{max}(T_{max}); and 5) The half-life ($t_{1/2}$).

RESULTS

Method development

During the development of a detection method for analytes A1, A5 and A6, multiple solvents were tested to find the optimal mobile phase. Compounds A1, A5 and A6 dissolved partially in water, but dissolved readily in methanol or acetonitrile. Acetonitrile was selected for better peak shape and compatibility with serum/brain protein precipitation. A5 and A6 were chosen as IS of A6, A1 and A5, respectively, because of their structural similarity. Selected reaction monitoring (SRM) acquisitions were used for sensitivity and extended dynamic range. The cone voltage and collision energy were optimized for A1, A5 and A6 and the IS by continuously infusing a mixture of the two. The optimum cone voltage was 30 V.

Matrix effects—There were no significant differences between the peaks generated by either the analytes extracted from the none-dosed ACSF, brain, and plasma or the analytes injected from water. The post-column infusion of 1 μg/ml A1, A5 or A6 showed no change of signal greater than 10% from sample matrix in their elution time windows.

Method validation

Selectivity—Selectivity was evaluated by analyzing non-dosed ACSF, brain, and plasma from three different mice. Individual samples were analyzed using LC-MS/MS conditions to prevent interference with A1, A5 and A6 as well as IS. No other endogenous peaks could be detected other than our analyte peaks, (Figure 2 & 3).

Linearity & LLOQ—The calibration curves were constructed by plotting the IS peak area ratio for analytes A1, A5 and A6 against the concentrations of the IS (A5 and A6). Each of the three calibrations curves (one for each matrix) were characterized by a linear segment and prepared in concentrations spanning 0.05–2.5 μg/ml. The regression equation for ACSF, plasma and brain for A1, A5 and A6 are listed in the (Table 1). Our LLOQ was 0.05 μg/ml from which a precision of < 10% RSD was observed.

Accuracy and precision—The intra-day and inter-day accuracy and precision values were determined after analyzing five replicates at three separate concentration levels (Table 2). Intra-day accuracy for all three analytes ranged from 91.5% to 112.5% and contained a

RSD range of 0.36% to 9.24%. All samples analyzed maintained a variability of <10% (RSD) (Table 2). These results support the accuracy, reliability and reproducibility of our method.

Stability—The stability of ABAD compounds were determined under different temperature and storage conditions (Table 3). A1, A5 and A6 standards were dissolved in methanol and were subjected short-term exposure at 25°C for 2 and 4 h long-term storage conditions were assessed at −20°C for twenty days. The displayed variability across all samples was less than 10% (RSD).

Pharmacokinetic profile of compound A1, A5 and A6—The LC-MS/MS method described above was used for the determination of A1, A5 and A6 in plasma, brain, and CSF for pharmacokinetic study. This is the first time such a method has been developed and utilized for this purpose. Figure 4 illustrates the plasma concentration–time profiles of A1, A5 and A6 with intravenous administration. Based on the initial concentration data, the pharmacokinetic parameters including the area under the plasma concentration-time curve during the period of observation ($AUC_{0\text{-}t}$), the area under the plasma concentration-time curve from zero to infinity ($AUC_{0\text{-}\infty}$) the maximum plasma concentration (C_{max}), the time to reach C_{max} (T_{max}) and the half-life ($t_{1/2}$) are shown in Table 4.

DISCUSSION

Molecular AD treatments need to cross the BBB to be effective. This restrictive membrane preserves the brain environment due to tight junctions between endothelial cells and transport mechanisms. It limits the access and distribution of molecules into the brain. Successful central nervous system (CNS) drugs have to cross the BBB, and this is often a limiting factor. Earlier studies in our laboratory have provided a series of small molecule benzothiazole phosphonates derivatives with low micromolar IC_{50} values against human ABAD [38]. These *in vitro* studies led us to choose the small molecule ABAD inhibitors (A1, A5 and A6) from this series for mouse pharmacokinetic studies. A detailed pharmacokinetics study of these new drugs candidates was therefore needed, and we have developed a new analytical LC–MS/MS approach to study the pharmacokinetic profiles of A1, A5 and A6 and describe it herein for mice plasma and brain samples after intravenous administration. The conditions for analysis and sample preparation were optimized, and the method was validated in terms of selectivity, sensitivity, accuracy, precision, and extraction recovery.

Pharmacokinetics provide new insights into the important role for understanding metabolism of drug action and is one of the most important techniques for elucidating the clinical efficacy or/and explaining and predicting a variety of events related to the efficacy [40–43]. The present study reveals a plasma and brain concentration–time curve for the three compounds. The detectable levels in brain suggested that the small molecule ABAD inhibitors (A1, A5 and A6) are able to cross the BBB.

CONCLUSION

To the best of our knowledge, this is the first report to validate a new LC-MS/MS analytical procedure for evaluating the pharmacokinetics of small molecule ABAD inhibitors (A1, A5 and A6) in mice. Our results clearly demonstrate that the LC–MS/MS method has excellent and satisfactory selectivity, sensitivity, linearity, precision, accuracy, and recovery. The separation of each analyte was conducted using a C-18 column along a methanol gradient. Each analyte was detected using tandem mass spectrometry-positive ion mode; followed by SRM experiments to observe the ions of each compound. Linearity was obtained using a concentration range of 0.05–2.5 μg/ml. The LLOQ and LLOD was 0.05 μg/ml. This specific and selective LC-MS/MS method was applied to a pharmacokinetic study after intravenous administration of A1, A5 and A6 and can be used in future pharmacokinetic studies. The compounds also efficiently cross the BBB and could therefore be effective AD drugs. The present *in vivo* pharmacokinetic studies of A1, A5 and A6 in mice provide valuable information for the systematic assessment and development of suitable dosage forms and clinical references concerning rational administration.

ACKNOWLEDGMENTS

This study was supported by grant awards (R37AG037319 and RO1NS65482) from the National Institute on Aging and National Institute of Neurological Disorder and Stroke and the University of Kansas Alzheimer's Disease Center (P30 AG035982). Partial instrument support NIH P20GM103418. The authors would like to thank Michael J. Baltezor, Colleen A. Flynn and Robert Winefield for their assistance in analyzing and interpreting the pharmacokinetic data using WinNonLin.

Abbreviations

AD	Alzheimer's disease
ABAD	Amyloid-beta binding alcohol dehydrogenase
Aβ	Amyloid beta peptide
ACSF	Artificial cerebrospinal fluid
BBB	Blood Brain Barrier
CNS	Central Nervous System
CSF	Cerebrospinal fluid
ESI	Electrospray ionization interface
FDA	Food and Drug Administration
HPLC	High-performance liquid chromatography
IS	Internal standard
LC-MS/MS	Liquid chromatography tandem mass spectrometry
LLOQ	Lower Limit of quantification
LLOD	Lower Limit of detection
QC	Quality control

SAR	Structure-activity relationship
SRM	Selected reaction monitoring
UPLC	Ultra Performance Liquid Chromatography

References

1. Du H, Guo L, Yan S, Sosunov AA, McKhann GM, Yan SS. Early deficits in synaptic mitochondria in an Alzheimer's disease mouse model. Proc Natl Acad Sci U S A. 2010; 107:18670–18675. [PubMed: 20937894]
2. Yao J, Irwin RW, Zhao L, Nilsen J, Hamilton RT, Brinton RD. Mitochondrial bioenergetic deficit precedes Alzheimer's pathology in female mouse model of Alzheimer's disease. Proc Natl Acad Sci U S A. 2009; 106:14670–14675. [PubMed: 19667196]
3. Caspersen C, Wang N, Yao J, Sosunov A, Chen X, Lustbader JW, Xu HW, Stern D, McKhann G, Yan SD. Mitochondrial Abeta: a potential focal point for neuronal metabolic dysfunction in Alzheimer's disease. FASEB J. 2005; 19:2040–2041. [PubMed: 16210396]
4. Reddy PH, Beal MF. Amyloid beta, mitochondrial dysfunction and synaptic damage: implications for cognitive decline in aging and Alzheimer's disease. Trends Mol Med. 2008; 14:45–53. [PubMed: 18218341]
5. Valla J, Berndt JD, Gonzalez-Lima F. Energy hypometabolism in posterior cingulate cortex of Alzheimer's patients: superficial laminar cytochrome oxidase associated with disease duration. J Neurosci. 2001; 21:4923–4930. [PubMed: 11425920]
6. Lunnon K, Ibrahim Z, Proitsi P, Lourdusamy A, Newhouse S, Sattlecker M, Furney S, Saleem M, Soininen H, Kloszewska I, Mecocci P, Tsolaki M, Vellas B, Coppola G, Geschwind D, Simmons A, Lovestone S, Dobson R, Hodges A, AddNeuroMed C. Mitochondrial dysfunction and immune activation are detectable in early Alzheimer's disease blood. J Alzheimers Dis. 2012; 30:685–710. [PubMed: 22466004]
7. Yan SD, Fu J, Soto C, Chen X, Zhu H, Al-Mohanna F, Collison K, Zhu A, Stern E, Saido T, Tohyama M, Ogawa S, Roher A, Stern D. An intracellular protein that binds amyloid-beta peptide and mediates neurotoxicity in Alzheimer's disease. Nature. 1997; 389:689–695. [PubMed: 9338779]
8. Manczak M, Calkins MJ, Reddy PH. Impaired mitochondrial dynamics and abnormal interaction of amyloid beta with mitochondrial protein Drp1 in neurons from patients with Alzheimer's disease: implications for neuronal damage. Hum Mol Genet. 2011; 20:2495–2509. [PubMed: 21459773]
9. Du H, Guo L, Zhang W, Rydzewska M, Yan S. Cyclophilin D deficiency improves mitochondrial function and learning/memory in aging Alzheimer disease mouse model. Neurobiol Aging. 2011; 32:398–406. [PubMed: 19362755]
10. Mao P, Manczak M, Calkins MJ, Truong Q, Reddy TP, Reddy AP, Shirendeb U, Lo HH, Rabinovitch PS, Reddy PH. Mitochondria-targeted catalase reduces abnormal APP processing, amyloid beta production and BACE1 in a mouse model of Alzheimer's disease: implications for neuroprotection and lifespan extension. Hum Mol Genet. 2012; 21:2973–2990. [PubMed: 22492996]
11. Wang X, Su B, Siedlak SL, Moreira PI, Fujioka H, Wang Y, Casadesus G, Zhu X. Amyloid-beta overproduction causes abnormal mitochondrial dynamics via differential modulation of mitochondrial fission/fusion proteins. Proc Natl Acad Sci U S A. 2008; 105:19318–19323. [PubMed: 19050078]
12. Takuma K, Fang F, Zhang W, Yan S, Fukuzaki E, Du H, Sosunov A, McKhann G, Funatsu Y, Nakamichi N, Nagai T, Mizoguchi H, Ibi D, Hori O, Ogawa S, Stern DM, Yamada K, Yan SS. RAGE-mediated signaling contributes to intraneuronal transport of amyloid-beta and neuronal dysfunction. Proc Natl Acad Sci U S A. 2009; 106:20021–20026. [PubMed: 19901339]
13. Eckert A, Hauptmann S, Scherping I, Rhein V, Muller-Spahn F, Gotz J, Muller WE. Soluble beta-amyloid leads to mitochondrial defects in amyloid precursor protein and tau transgenic mice. Neurodegener Dis. 2008; 5:157–159. [PubMed: 18322377]

14. Manczak M, Anekonda TS, Henson E, Park BS, Quinn J, Reddy PH. Mitochondria are a direct site of A beta accumulation in Alzheimer's disease neurons: implications for free radical generation and oxidative damage in disease progression. Hum Mol Genet. 2006; 15:1437–1449. [PubMed: 16551656]
15. Lustbader JW, Cirilli M, Lin C, Xu HW, Takuma K, Wang N, Caspersen C, Chen X, Pollak S, Chaney M, Trinchese F, Liu S, Gunn-Moore F, Lue LF, Walker DG, Kuppusamy P, Zewier ZL, Arancio O, Stern D, Yan SS, Wu H. ABAD directly links Abeta to mitochondrial toxicity in Alzheimer's disease. Science. 2004; 304:448–452. [PubMed: 15087549]
16. Valasani KR, Chaney MO, Day VW, Shidu Yan S. Acetylcholinesterase inhibitors: structure based design, synthesis, pharmacophore modeling, and virtual screening. J Chem Inf Model. 2013; 53:2033–2046. [PubMed: 23777291]
17. Yang SY, He XY, Schulz H. Multiple functions of type 10 17beta-hydroxysteroid dehydrogenase. Trends Endocrinol Metab. 2005; 16:167–175. [PubMed: 15860413]
18. He XY, Merz G, Yang YZ, Pullakart R, Mehta P, Schulz H, Yang SY. Function of human brain short chain L-3-hydroxyacyl coenzyme A dehydrogenase in androgen metabolism. Biochim Biophys Acta. 2000; 1484:267–277. [PubMed: 10760475]
19. He XY, Merz G, Mehta P, Schulz H, Yang SY. Human brain short chain L-3-hydroxyacyl coenzyme A dehydrogenase is a single-domain multifunctional enzyme. Characterization of a novel 17beta-hydroxysteroid dehydrogenase. J Biol Chem. 1999; 274:15014–15019. [PubMed: 10329704]
20. He XY, Schulz H, Yang SY. A human brain L-3-hydroxyacyl-coenzyme A dehydrogenase is identical to an amyloid beta-peptide-binding protein involved in Alzheimer's disease. J Biol Chem. 1998; 273:10741–10746. [PubMed: 9553139]
21. Ofman R, Ruiter JP, Feenstra M, Duran M, Poll-The BT, Zschocke J, Ensenauer R, Lehnert W, Sass JO, Sperl W, Wanders RJ. 2-Methyl-3-hydroxybutyryl-CoA dehydrogenase deficiency is caused by mutations in the HADH2 gene. Am J Hum Genet. 2003; 72:1300–1307. [PubMed: 12696021]
22. He XY, Yang YZ, Peehl DM, Lauderdale A, Schulz H, Yang SY. Oxidative 3alpha-hydroxysteroid dehydrogenase activity of human type 10 17beta-hydroxysteroid dehydrogenase. J Steroid Biochem Mol Biol. 2003; 87:191–198. [PubMed: 14672739]
23. Ivell R, Balvers M, Anand RJ, Paust HJ, McKinnell C, Sharpe R. Differentiation-dependent expression of 17beta-hydroxysteroid dehydrogenase, type 10, in the rodent testis: effect of aging in Leydig cells. Endocrinology. 2003; 144:3130–3137. [PubMed: 12810569]
24. He XY, Wegiel J, Yang YZ, Pullarkat R, Schulz H, Yang SY. Type 10 17beta-hydroxysteroid dehydrogenase catalyzing the oxidation of steroid modulators of gamma-aminobutyric acid type A receptors. Mol Cell Endocrinol. 2005; 229:111–117. [PubMed: 15607535]
25. Takuma K, Yao J, Huang J, Xu H, Chen X, Luddy J, Trillat AC, Stern DM, Arancio O, Yan SS. ABAD enhances Abeta-induced cell stress via mitochondrial dysfunction. Faseb J. 2005; 19:597–598. [PubMed: 15665036]
26. Yan Y, Liu Y, Sorci M, Belfort G, Lustbader JW, Yan SS, Wang C. Surface plasmon resonance and nuclear magnetic resonance studies of ABAD-Abeta interaction. Biochemistry. 2007; 46:1724–1731. [PubMed: 17253767]
27. Rao VK, Carlson EA, Yan SS. Mitochondrial permeability transition pore is a potential drug target for neurodegeneration. Biochim Biophys Acta. 2013
28. Yan SD, Stern DM. Mitochondrial dysfunction and Alzheimer's disease: role of amyloid-beta peptide alcohol dehydrogenase (ABAD). Int J Exp Pathol. 2005; 86:161–171. [PubMed: 15910550]
29. Valasani KR, Vangavaragu JR, Day VW, Yan SS. Structure Based Design, Synthesis, Pharmacophore Modeling, Virtual Screening, and Molecular Docking Studies for Identification of Novel Cyclophilin D Inhibitors. J Chem Inf Model. 2014
30. Yan SD, Shi Y, Zhu A, Fu J, Zhu H, Zhu Y, Gibson L, Stern E, Collison K, Al-Mohanna F, Ogawa S, Roher A, Clarke SG, Stern DM. Role of ERAB/L-3-hydroxyacyl-coenzyme A dehydrogenase type II activity in Abeta-induced cytotoxicity. J Biol Chem. 1999; 274:2145–2156. [PubMed: 9890977]

31. Xie Y, Deng S, Chen Z, Yan S, Landry DW. Identification of small-molecule inhibitors of the Abeta-ABAD interaction. Bioorg Med Chem Lett. 2006; 16:4657–4660. [PubMed: 16781151]
32. Somogyi G, Nishitani S, Nomi D, Buchwald P, Prokai L, Bodor N. Targeted drug delivery to the brain via phosphonate derivatives - I. Design, synthesis and evaluation of an anionic chemical delivery system for testosterone. International Journal of Pharmaceutics. 1998; 166:15–26.
33. Somogyi G, Buchwald P, Nomi D, Prokai L, Bodor N. Targeted drug delivery to the brain via phosphonate derivatives - II. Anionic chemical delivery system for zidovudine (AZT). International Journal of Pharmaceutics. 1998; 166:27–35.
34. Somogyi G, Buchwald P, Bodor N. Targeted drug delivery to the central nervous system via phosphonate derivatives (Anionic delivery system for testosterone). Pharmazie. 2002; 57:135–137. [PubMed: 11878190]
35. Rao VK, Reddy SS, Krishna BS, Reddy CS, Reddy NP, Reddy TCM, Raju CN, Ghosh SK. Design, Synthesis and Anti Colon Cancer Activity Evaluation of Phosphorylated Derivatives of Lamivudine (3TC). Letters in Drug Design & Discovery. 2011; 8:59–64.
36. Rao VK, Rao AJ, Reddy SS, Raju CN, Rao PV, Ghosh SK. Synthesis, spectral characterization and biological evaluation of phosphorylated derivatives of galanthamine. European Journal of Medicinal Chemistry. 2010; 45:203–209. [PubMed: 19853328]
37. Valasani KR, Hu G, Chaney MO, Yan SS. Structure-based design and synthesis of benzothiazole phosphonate analogues with inhibitors of human ABAD-Abeta for treatment of Alzheimer's disease. Chem Biol Drug Des. 2013; 81:238–249. [PubMed: 23039767]
38. Koteswara Rao Valasani QS, Gang Hu, Jianping Li, Fang Du, Yaopeng Guo, Carlson Emily A, Xueqi Gan, Yan Shirley ShiDu. Identification of Human ABAD Inhibitors for Rescuing Abeta-Mediated Mitochondrial Dysfunction. Current Alzheimer Research. 2014; 11:000–000.
39. Guidance for Industry-Bioanalytical Method Validation. US Food and Drug Administration. 2001
40. Lv J, Pan L, Ye Y, Zhou Y. A sensitive and selective RP-HPLC method for simultaneous determination of picroside-I and picroside-II in rat plasma and its application in pharmacokinetics studies. J Sep Sci. 2007; 30:2466–2472. [PubMed: 17628865]
41. Samanidou VF, Nika MK, Papadoyannis IN. Development of an HPLC method for the monitoring of tricyclic antidepressants in biofluids. J Sep Sci. 2007; 30:2391–2400. [PubMed: 17625794]
42. Cheng S, Qiu F, Wang S, He J. HPLC analysis and pharmacokinetics of icariin in rats. J Sep Sci. 2007; 30:1307–1312. [PubMed: 17623472]
43. Xue YJ, Yan JH, Arnold M, Grasela D, Unger S. Quantitative determination of BMS-378806 in human plasma and urine by high-performance liquid chromatography/tandem mass spectrometry. J Sep Sci. 2007; 30:1267–1275. [PubMed: 17623467]

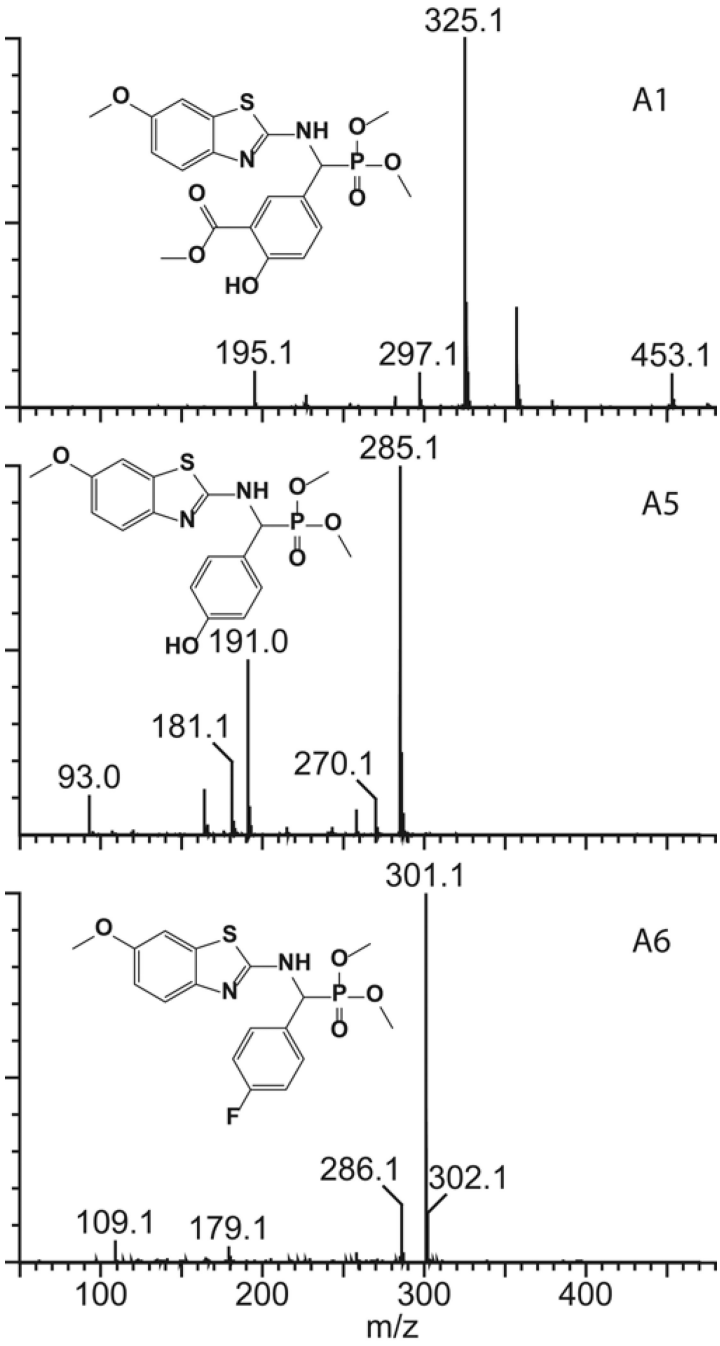

Figure 1.

Tandem mass spectrums of compounds A1 ($[M+H]^+$ = 453), A5 ($[M+H]^+$ = 395), & A6 ($[M+H]^+$ = 397), after activation of $[M+H]^+$ at 30 V. The base peak fragments were the product ion used in SRM transitions. Cone voltage was 30 V.

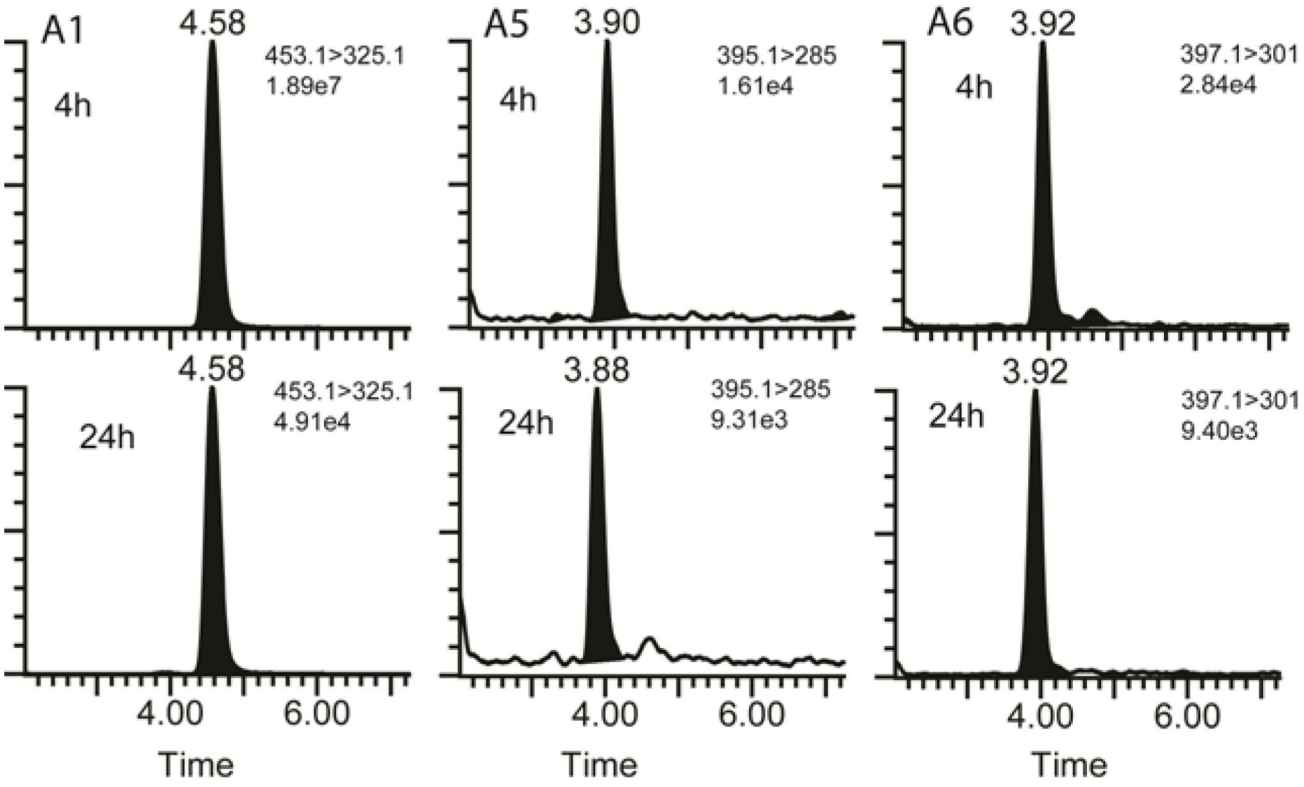

Figure 2.

HPLC/SRM chromatograms of A1, A5 & A6 compounds; mouse CSF samples collected after 4h & 24h post intravenous injection of 10 mg/kg A1, A5 & A6, respectively. The representative chromatograms clearly shows that these three compounds when dosed individually penetrates the biological membrane i.e., BBB and enters the target organ. Sample preparation for 20µl of CSF was performed using 20µL of methanol (including 1µg/ml IS), 50% organic and 50% aqueous solution.

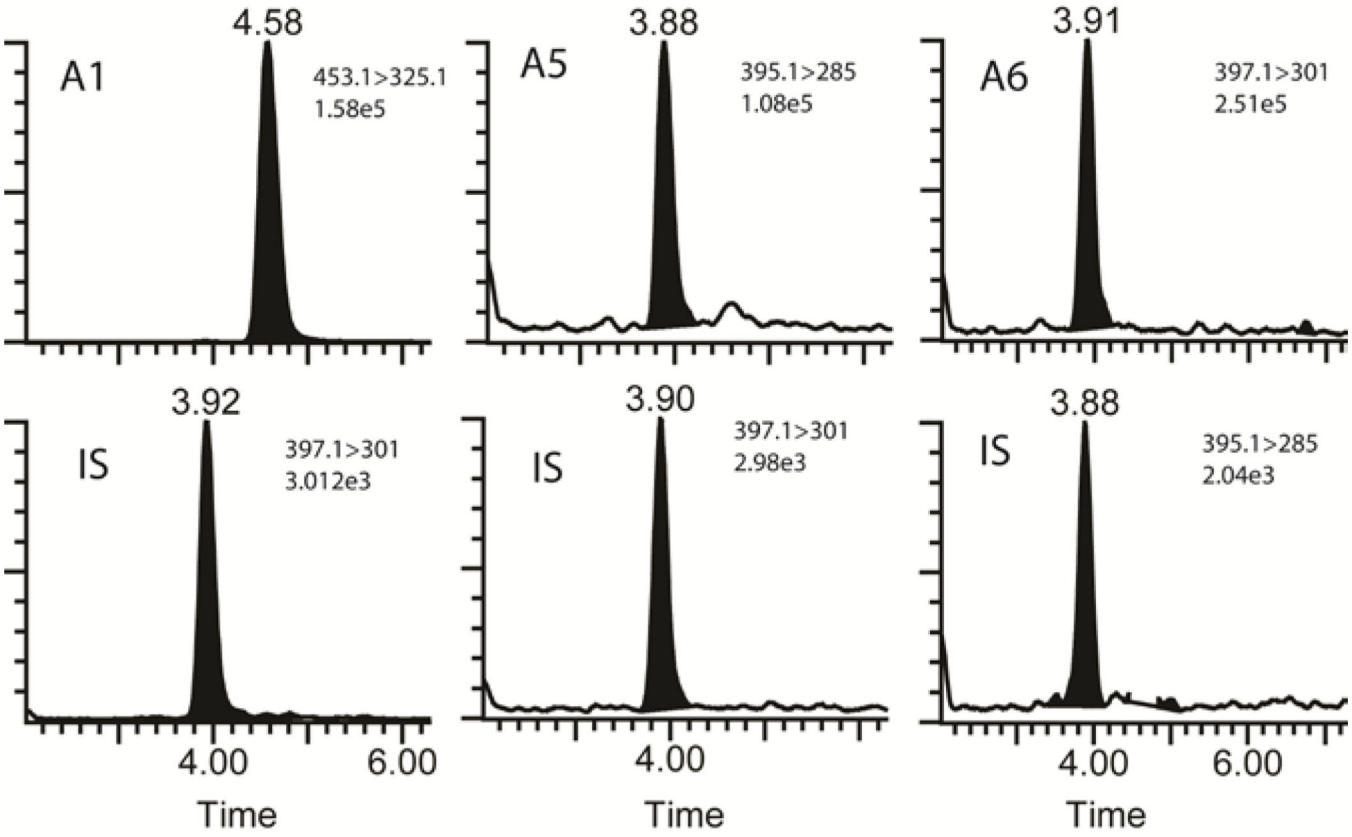

Figure 3.

HPLC/SRM chromatograms of A1, A5 & A6 compounds; mouse brain samples collected at 30min after intravenous injection of 10 mg/kg A1, A5 & A6, respectively. The representative chromatograms clearly shows that these three compounds when dosed individually penetrates the biological membrane i.e., BBB and enters the brain. Sample preparation for 100mg brain was performed using 200µl of 50/50 methanol/water (including 6µg/ml IS).

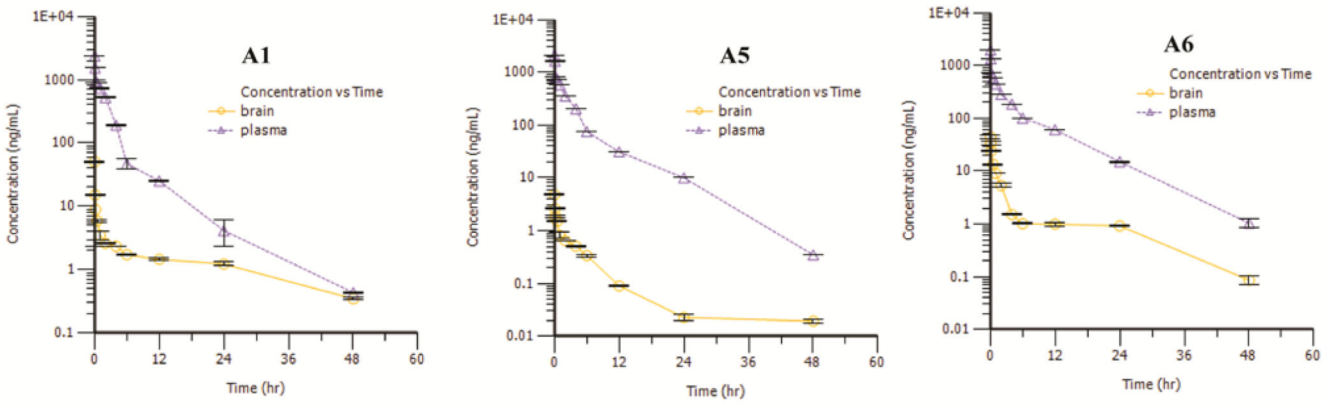

Figure 4.

Mean plasma and brain concentration-time curves of compounds A1, A5 & A6 after 10 mg/kg intravenous injection in mice. Each value is the mean ± SD of three determinations for brain (circles) and plasma (triangle).

Table 1

Linear regression calibration equations from spiked ACSF, Plasma, Brain (n = 5) Area anlayte/Area internal standard.

	Compound A1	Compound A5	Compound A6
ACSF			
Day-1	y = 1.9104*x*+0.2883 (r^2 = 0.9989)	y = 4.2853*x*+0.3385 (r^2 = 0.9987)	y = 0.0274*x*+0.0346 (r^2 = 0.9948)
Day-2	y = 1.859*x*+ 0.1983 (r^2 = 0.9950)	y = 4.7043*x*+0.1764 (r^2 = 0.9936)	y = 0.0277*x*+0.0395 (r^2 = 0.9820)
Day-3	y = 1.8361*x*+0.1761 (r^2 = 0.9919)	y = 4.4399x+0.2693 (r^2 = 0.9859)	y = 0.0268*x*+0.0354 (r^2 = 0.9839)
Plasma			
Day-1	y = 6.8079*x* +0.6036 (r^2 = 0.9808)	y = 18.2874*x*+0.3274 (r^2 = 0.9929)	y = 19.2733*x*+0.3176 (r^2 = 0.9968)
Day-2	y = 6.8628*x* +0.8166 (r^2 = 0.9882)	y = 17.9314*x*+0.0688 (r^2 = 0.9941)	y = 19.0504x+0.5253 (r^2 = 0.9709)
Day-3	y = 6.9525*x*+0.9087 (r^2 = 0.9854)	y = 19.3519*x*+0.2756 (r^2 = 0.9788)	y = 19.3519*x*+0.2756 (r^2 = 0.9788)
Brain			
Day-1	y = 1.4924*x* +0.0471 (r^2 = 0.9905)	y = 5.0012*x*+0.0643 (r^2 = 0.9922)	y = 2.4517*x*+0.2544 (r^2 = 0.9926)
Day-2	y = 1.5079x +0.3429 (r^2 = 0.9975)	y = 5.2436*x*+0.0597 (r^2 = 0.9871)	y = 2.7797*x*+0.3781 (r^2 = 0.9915)
Day-3	y = 1.4983x +0.1586 (r^2 = 0.9845)	y = 5.1974*x*+0.0625 (r^2 = 0.9918)	y = 2.6885*x*+0.2814 (r^2 = 0.9964)

Table 2

Intra- and inter-day accuracy and precision for compounds **A1**, **A5** and **A6** in mouse plasma, brain and ACSF (n = 5). Accuracy determined as Signal from spiked matrix/ Signal from methanol/water "pure" standard.

		Plasma				Brain				ACSF			
		Inter-day		Intra-day		Inter-day		Intra-day		Inter-day		Intra-day	
Cmpd	Nominal con.(ng/ml)	Accuracy (%)	Precision (RSD, %)	Accuracy (%)	Precision (RSD, %)	Accuracy (%)	Precision (RSD, %)	Accuracy (%)	Precision (RSD, %)	Accuracy (%)	Precision (RSD, %)	Accuracy (%)	Precision (RSD, %)
A1	0.05	108.602	9.2	108.224	6.4	112.463	5.6	106.8	6.7	108.560	5.8	108.680	6.2
A1	0.875	98.859	1.1	99.097	1.1	99.704	0.7	99.322	1.1	99.054	1.4	99.054	0.9
A1	2.5	101.423	1.5	98.118	4.4	100.522	0.6	99.756	2.5	99.723	0.8	102.331	2.6
A5	0.05	95.231	7.8	100.076	5.8	91.491	5.2	91.491	5.6	94.467	6.1	94.467	4.2
A5	0.875	100.337	0.6	100.651	0.8	101.013	2.1	100.932	1.4	101.563	2.5	101.563	2.6
A5	2.5	100.527	0.1	98.683	2.6	98.785	1.1	100.195	2.9	98.461	2.1	95.383	3.3
A6	0.05	101.288	7.2	101.288	5.8	101.553	6.4	101.553	4.8	96.854	4.7	95.298	5.9
A6	0.875	102.621	0.7	102.514	0.8	102.006	0.6	102.00	0.3	102.81	1.4	101.925	1.7
A6	2.5	102.101	5.3	98.118	3.1	102.442	0.8	101.927	2.3	101.386	1.3	100.996	2.6

Table 3

Stability of compounds **A1**, **A5** and **A6** under various conditions (n = 5) in in mouse plasma, brain and ACSF. Recovery determined as Signal from spiked matrix/ Signal from methanol/water “pure” standard.

Storage conditions	Concen. (ng/ml) nominal	ACSF (Accuracy ± RSD (%))			Plasma (Accuracy ± RSD (%))			Brain (Accuracy ± RSD (%))		
		A1	A5	A6	A1	A5	A6	A1	A5	A6
Freeze-thaw stability	0.05	109.68±7.1	97.4±1.6	103.72±6.1	114.8±4.2	108.0±8.2	110.84±4.3	104.8±1.2	99.92±5.2	111.44±5.2
	0.875	99.51±0.7	99.56±0.5	99.73±0.7	99.88±6.8	99.88±6.8	99.98±6.4	99.71±7.1	99.81±6.9	100.41±8.1
	2.5	104.81±3.6	97.68±2.6	103.42±0.9	100.4±2.1	100.84±9.1	100.49±8.1	104.4±5.6	99.36±8.4	101.92±7.9
Stability at room temperature (2 h)	0.05	103.48±5.7	99.04±6.6	102.24±4.6	103.52±9.2	99.84±7.8	106.92±7.2	107.2±5.6	95.92±5.2	103.44±6.4
	0.875	99.62±1.3	100.5±2.5	100.50±1.4	99.42±1.1	99.31±0.6	100.31±0.7	100.2±0.71	99.98±2.1	99.72±0.5
	2.5	100.1±0.7	99.53±2.2	100.43±1.2	101.72±1.4	101.62±0.2	101.14±5.3	87.46±1.2	99.86±1.1	100.72±0.8
Stability at room temperature (4 h)	0.05	103.74±6.4	94.12±3.1	98.03±7.3	99.56±5.5	110.12±5.9	102.56±5.1	100.93±9.1	101.24±4.3	105.7±3.1
	0.875	100.51±1.4	99.28±3.9	98.62±0.9	99.27±1.5	99.22±0.89	100.04±0.5	100.41±0.8	99.68±0.9	100.06±0.2
	2.5	104.54±2.1	96.42±5.2	100.04±2.8	98.40±6.6	97.82±3.4	100.54±0.6	102.21±3.2	101.28±5.7	102.82±2.6
Stability at −20°C (20days)	0.05	103.56±6.6	96.04±3.6	101.52±5.7	106.4±4.3	104.8±3.6	105.24±5.1	97.27±5.6	101.0±7.2	103.84±5.2
	0.875	100.01±0.1	98.69±1.2	99.78±2.7	100.3±0.6	100.56±1.1	100.26±1.2	98.98±1.7	100.05±1.1	99.98±0.3
	2.5	103.33±4.9	96.39±2.4	96.60±3.7	100.62±5.5	99.82±4.3	99.49±3.2	97.12±3.2	98.24±2.1	98.60±3.5

Table 4

Pharmacokinetics of parameters **A1**, **A5** and **A6** after intravenous injection of 10 mg/kg in mice

Compound	Matrix	$t_{1/2}$ (h)	Tmax (h)	C_{max} (ng/mL)	$AUC_{(0–48)}$ (h*ng/mL)	$AUC_{(0-\infty)}$ (h*ng/mL)
A1	brain	17.1	0.03	50.7	66.5	75.1
A1	plasma	6.2	0.03	2370.1	3027.8	3031.6
A5	brain	8.3	0.03	4.8	6.9	7.1
A5	plasma	5.5	0.03	2129.4	2862.6	2865.4
A6	brain	11.4	0.03	44.3	64.0	65.4
A6	plasma	6.1	0.03	1982.7	2983.9	2993.0